Large-scale Simulations of Adhesion in Dense Polymer Melts

Scott W. Sides, Gary S. Grest, and Mark J. Stevens
Sandia National Laboratories, Albuquerque, New Mexico 87185-1411

ABSTRACT

We study adhesion between a polymer melt and substrate due to tethered chains on the substrate surface. We have performed extensive molecular dynamics simulations to study the effect of tethered chain density (Σ), tethered chain length ($N_{\rm t}$) and tensile pull velocity (v) on the adhesive failure mechanisms. We incorporate a simple breaking model to study the scission of the tethered chains as they are pulled from the melt. We observe a crossover from pure chain pullout at short $N_{\rm t}$ and small v, to chain scission as $N_{\rm t}$ and v are increased. The value of $N_{\rm t}$ for which this crossover occurs is comparable to the entanglement length.

Keywords: polymer, adhesion, molecular dynamics, simulation

1. INTRODUCTION

Adhesion at polymer interfaces is relevant in either the mixing of two immiscible homopolymers (A+B) or attaching a homopolymer melt to a hard surface (A+substrate). In both cases, the addition of a third component can increase the entanglements at a polymer interface. For the first case, the extra component is a block copolymer made of the A and B species. For the latter case, the extra component is a layer of the A species which is chemically end-grafted onto the substrate. These tethered polymer layers, or brushes are relevant in such applications as colloidal stabilization [1,2], filler modification of polymeric materials and lubrication [3]. Substrate-tethered polymers can also enhance adhesion i. e. increase the mechanical work needed to break an adhesive bond.

Two key parameters characterizing this system are the length ($N_{\rm t}$) and the areal density (Σ) of the tethered chains. Adhesion enhancement due to a tethered polymer layer shows a surprising non-monotonic behavior as a function of $N_{\rm t}$ and Σ. The work of adhesion first increases for small values of $N_{\rm t}$ and Σ, then decreases once either of these parameters is increased beyond a critical value, due to the phase behavior of the end-tethered chains in contact with a long polymer melt [4–7]. This non-monotonic behavior has been observed by Kramer and co-workers in glassy polymers [8–12] and Léger and co-workers in elastomeric materials [7,13]. However, the interplay between the microscopic failure mechanisms of tethered chain pullout, scission and crazing are not fully understood, partly due to the difficulty of direct experimental observation of these phenomena. Molecular dynamics (MD) simulations of fracture in highly crosslinked systems [14] and crazing [15,16] have helped to elucidate the crossover from adhesive to cohesive failure of polymer adhesives near walls *without* end-tethered chains. Simulations of tethered chains on small, highly simplified models in 2D have been performed [17,18], but were unable to study the effects of chain scission in particular. In this letter we present the first, large-scale simulations to study the adhesive failure mechanisms of end-tethered chains in contact with an entangled polymer melt.

2. MD MODEL/METHOD

We perform continuous-space, molecular dynamics (MD) simulations on a coarse-grained model of polymer chains. The polymers are represented by attaching N spherical beads of mass m with breakable springs. Bead trajectories are obtained by stepwise integration of Newton's equations of motion (EOM) using a velocity-Verlet [19] algorithm with a time step Δt=0.006τ, where τ=$\sigma(m/\epsilon)^{1/2}$, with σ and ϵ setting the length and energy scales respectively. The EOM includes terms for a weak stochastic force and a viscous drag force with a coefficient on the viscous force term of $0.5\tau^{-1}$ [20]. The addition of these two forces to the EOM effectively couples the system to a heat bath. Each nonbonded pair of monomers interacts through a standard (12-6) Lennard-Jones interaction $U_{\rm LJ}(r)$, truncated at r_c=2.2σ.

To study the effect of chain scission on adhesion, the standard finite extensible non-linear elastic (FENE) potential [20] is altered to allow for broken bonds along a polymer chain. The total non-breakable potential $U_{\rm nb}(r)$ (including the FENE potential), between two adjacent beads a distance r apart on the same chain takes the form

$$U_{\rm nb}(r) = \begin{cases} U_{\rm LJ}(r) + -0.5KR_o^2 \ln\left[1-\left(\frac{r}{R_o}\right)^2\right] & r < R_o \\ \infty & r > R_o \end{cases}$$

while the breakable potential $U_{\rm b}(r)$, takes the form

$$U_{\rm b}(r) = \begin{cases} U_{\rm LJ}(r) + kr^4\left[(r-r_1)(r-r_2)\right] + U_c & r < r_{\rm br} \\ 0 & r > r_{\rm br} \end{cases}$$

with $r_{\rm br}$ the length at which a bond along the chain is considered broken. The remaining parameters in $U_{\rm b}(r)$ are k=$-409.12\epsilon/\sigma^6$, r_1=1.2σ, r_2=1.219σ and

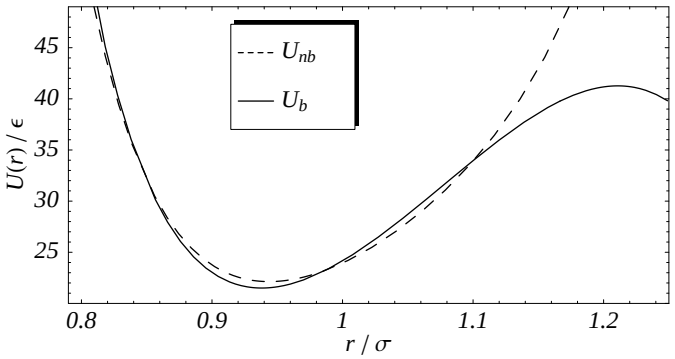

FIG. 1. Comparison of the breaking potential $U_{\rm b}(r)$ and the non-breakable potential $U_{\rm nb}(r)$ using a standard FENE potential.

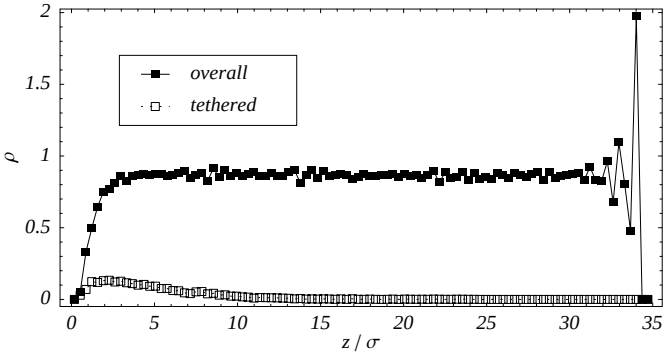

FIG. 2. Density profiles $\rho(z)$ for all monomers in the system (filled square) and monomers belonging to the tethered chains (open square). The data shown is for T=1.0$\epsilon/k_{\rm B}$, $N_{\rm t}$=100 and Σ=0.008σ^{-2}.

U_c=42.059ϵ which result from fitting $U_{\rm b}(r)$ to a standard FENE potential [20] such that $r_{\rm br}$=1.21σ and the barrier to bond breaking is $\Delta U_{\rm b} \approx 20 k_{\rm B}T$. The FENE parameters used in the fit of the breakable potential are K=30.0ϵ/σ^2 and R_o=1.25σ. Figure 1 compares the standard non-breakable potential to the breakable potential used in this study. The form of $U_{\rm b}(r)$ allows for two extrema in the bond potential; one stable, global minimum near the LJ potential energy minimum, and one local maximum near $r_{\rm br}$ where the bond force becomes zero. This allows bonds to be removed safely from the force calculation without causing large recoil velocities on the resulting chain ends.

Figure 2 shows the monomer density profile for a system before pulling and consists of approximately 10^5 particles with with $N_{\rm t}$=100. Our largest systems contain close to 10^6 particles. The density profile is a function of z with the z axis normal to both walls. Periodic boundary conditions used in the x and y directions. The left wall at z=0 has tethered chains attached while the right wall has no tethered chains. The tensile pull is achieved by moving only the left wall at constant velocity. For speed and simplicity, the wall interaction with the chains is modeled as an integrated LJ potential. The interaction strength of the left wall is set to be sufficiently strong so that no adhesive failure occurs on the right wall during pulling. The interaction of the left wall with the melt has a very weak attractive component, so that the adhesion enhancement due to the tethered chains may be studied independently of the adhesion to the bare wall. The size of the simulation cell in the z direction is set to be approximately three times the radius of gyration of the tethered chains prior to pulling. Several factors need to be considered to construct and equilibrate appropriate starting states. To avoid the difficulties in constructing the correct chain configurations for the various wet brush regimes we restrict the present study to areal densities Σ in the so-called "mushroom regime" [4,5]. In this regime each tethered chain does not interact directly with other tethered chains and may be constructed as a Gaussian chain. So, for each system of a given $N_{\rm t}$ and Σ, all chains are constructed as random walks with the correct radius of gyration and the tethered chains are attached to the substrate wall in random locations. A soft potential is used to remove overlaps and the size of the simulation cell is adjusted until the pressure $P \approx 0$ resulting in an overall monomer density of $\rho \approx 0.85\sigma^{-3}$. For all simulations, the number of beads in each of the melt chains is N_m=2500 and the number of tethered chains is $n_{\rm t}$=30. Most of the simulations are performed with T=1.0$\epsilon/k_{\rm B}$, which is well above the glass transition temperature $T_{\rm g}$=0.5 − 0.6$\epsilon/k_{\rm B}$ [15]. Simulations are performed using the massively parallel MD code LAMMPS [21], developed at Sandia and run on the ASCI Red Teraflop machine and Computational Plant (Cplant $^{\rm TM}$) clusters.

3. RESULTS

During a pull simulation we measure the remaining length of the tethered chains and the work done by the left wall. Figure 3 shows the integrated work over time W, as a function of time for $N_{\rm t}$=100, 250 and compares the non-breakable and breakable potentials. The data shown in Fig. 3 are for v=0.0167$\sigma\tau^{-1}$, T=1.0$\epsilon/k_{\rm B}$ and Σ=0.008σ^{-2}. The plateau in W signifies the complete debonding of the pulling surface from the entangled melt. For the larger $N_{\rm t}$ the slope of W in the plateau region does not vanish because finite work is done pulling the remaining parts of the tethered chains due to the presence of an effective solvent as a result of the heat bath

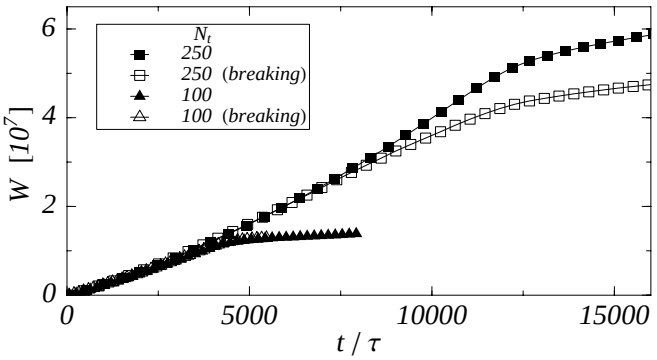

FIG. 3. Total integrated work vs. time for breakable and unbreakable chains. The data are for $N_{\rm t}$=100, 250, v=0.0167$\sigma\tau^{-1}$, T=1.0$\epsilon/k_{\rm B}$ and Σ=0.008σ^{-2}. For each tethered chain length, W is plotted for a sufficiently long time such that the tethered chains have either completely pulled out or each of the attached chains has broken.

algorithm in the EOM. Clearly, surfaces with longer tethered chains require more work to completely pull away from the adjacent polymer melt than do short chains. For $N_{\rm t}$=100, the data from the non-breakable and breakable potentials is nearly identical. For the longer tethered chains of $N_{\rm t}$=250, the potentials give significantly different results. This shows that longer tethered chains are subject to sufficiently large stresses that cause them to break.

Figure 4, which shows the average fractional length of remaining tethered chains $\langle F\rangle$ versus $N_{\rm t}$. All the data in Fig. 4 is obtained using the breakable potential. If $N^f_{{\rm t},i}$ is defined to be length of the ith tethered chain at the end of a pull simulation then

$$\langle F\rangle = \frac{1}{n_{\rm t}}\sum_i^{n_{\rm t}} \frac{N^f_{{\rm t},i}}{N_{\rm t}} \ .$$

The value of $\langle F\rangle$ quantifies the length of the tethered chains still attached to the surface at the end of a pull. $\langle F\rangle$=1 corresponds to pure chain pullout and $\langle F\rangle$=0 to pure chain scission. The filled symbols in Fig. 4 represent data for two velocities at Σ=0.008σ^{-2} and show an adhesive failure mechanism of almost pure chain pullout for $N_{\rm t} \leq 100$. At $N_{\rm t} \sim 100$ there is a crossover to a failure mechanism with greater amounts of chain scission as $N_{\rm t}$ increases. The entanglement length calculated from the plateau modulus for this model has been estimated by Pütz et al. [22] to be $N_{\rm e} \approx 74$. Thus, the crossover value corresponds to approximately $1.5N_{\rm e}$. However other calculations [23] suggest that $N_{\rm e}$ may increase in the vicinity of a hard wall. For a given v and T, the amount of chain scission appears to saturate for $N_{\rm t} \gg N_{\rm e}$, so the average length of the remaining tethered chains approaches a constant value. The open triangles in Fig. 4 show data for v=0.0167$\sigma\tau^{-1}$ and Σ=0.002σ^{-2} and illustrate that $\langle F\rangle$ is independent of areal density. This confirms our estimates of Σ which place the system near the "mushroom regime". The velocity dependence of chain scission is illustrated by the inset in Fig. 4 which shows $\langle F\rangle$ over three decades in pulling velocity. The amount of chain scission clearly decreases with decreasing pull velocity.

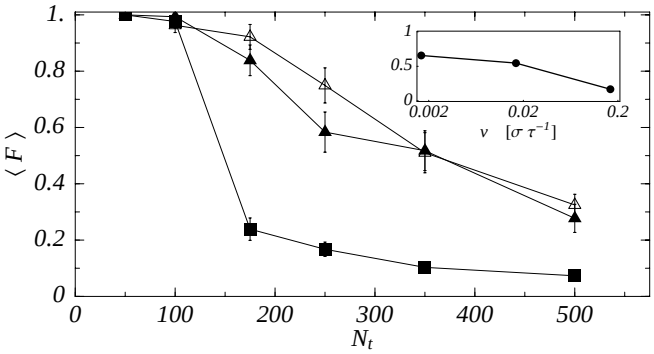

FIG. 4. Average fractional length of remaining tethered chains $\langle F\rangle$ vs. initial tethered chain length $N_{\rm t}$. The data shown are all for uncrosslinked systems at T=1.0$\epsilon/k_{\rm B}$. The symbols denote v=0.167$\sigma\tau^{-1}$, Σ=0.008σ^{-2} (filled square), v=0.0167$\sigma\tau^{-1}$, Σ=0.008σ^{-2} (filled triangle), and v=0.0167$\sigma\tau^{-1}$, Σ=0.002σ^{-2} (open triangle). Inset: $\langle F\rangle$ vs. tensile pull velocity v for T=1.0$\epsilon/k_{\rm B}$, $N_{\rm t}$=250 and Σ=0.008σ^{-2}.

4. CONCLUSION

In conclusion, we performed the first large-scale MD simulations to study the effects of end-tethered chains on adhesion in a 3D, realistic polymer model. Data is presented which illustrates a crossover from pure chain pullout to increasing chain scission which depends on $N_{\rm t}$ and v. The value of $N_{\rm t}$ for which this crossover occurs is near the entanglement length N_e for this model. Experiments on the fracture properties of glassy polymers reinforced by block copolymer additives report a large increase in the work of adhesion when the molecular weight of the copolymer increases beyond the entanglement length. The data suggest this increase is due to crazing which is not seen in our simulations because of the weak attractive wall interaction and temperatures above the glass transition. In experiments on glassy polymers, entangled tethered chains presumably transfer enough stress into the melt to initiate crazing. By analogy with our simulations, tethered chain lengths greater than the entanglement length are subject to sufficient stress to break bonds along the chains. Further work is needed to investigate the effect of tethered chains specifically on

crazing mechanisms and the possible roles of chain pull-out and scission on craze failure. Work is proceeding to extend simulations to include non-zero bond bending and torsional interactions as well as realistic potentials for materials like PDMS.

Sandia is a multiprogram laboratory operated by Sandia Corporation, a Lockheed Martin Company, for the United States Department of Energy under Contract DE-AC04-94AL85000.

---

[1] D. H. Napper, *Polymeric Stabilization of Colloidal Dispersions* (Academic, London, 1983).

[2] W. B. Russell, D. A. Saville, and W. R. Schowalter, *Colloidal Dispersions* (Cambridge University Press, Cambridge, 1989).

[3] J. Klein, Ann. Rev. Mat. Sci. **26**, 581 (1996).

[4] P. G. deGennes, Macromolcules **13**, 1069 (1980).

[5] M. Aubouy, G. H. Fredrickson, P. Pincus, and E. Raphaël, Macromolecules **28**, 2979 (1995).

[6] G. S. Grest, J. Chem. Phys. **105**, 5532 (1996).

[7] L. Léger, E. Raphaël, and H. Hervet, in *Advances In Polymer Science*, edited by S. Granick (Springer, Berlin, 1999), Vol. 138, p. 185.

[8] C. Creton, E. J. Kramer, and G. Hadziioannou, Macromolecules **24**, 1846 (1991).

[9] J. Washiyama, E. J. Kramer, C. F. Creton, and C.-Y. Hui, Macromolecules **27**, 2019 (1994).

[10] E. J. Kramer *et al.*, Faraday Discuss. **98**, 31 (1994).

[11] L. Norton *et al.*, Macromolecules **28**, 1999 (1995).

[12] C.-A. Dai, E. J. Kramer, J. Washiyama, and C.-Y. Hui, Macromolecules **29**, 7536 (1996).

[13] M. Deruelle, L. Léger, and M. Tirrell, Macromolecules **28**, 7419 (1995).

[14] M. J. Stevens, Macromolecules, in press .

[15] A. R. C. Baljon and M. O. Robbins, Science **271**, 482 (1996).

[16] D. Gersappe and M. O. Robbins, Euro. Phys. Lett. **48**, 150 (1999).

[17] G. T. Pickett, D. Jasnow, and A. C. Balazs, Phys. Rev. Lett. **77**, 671 (1996).

[18] M. Sabouri-Ghomi, S. Ispolatov, and M. Grant, Phys. Rev. E **60**, 4460 (1999).

[19] M. Allen and D. Tildesley, *Computer Simulation of Liquids* (Clarendon, Oxford, 1987).

[20] K. Kremer and G. S. Grest, J. Chem. Phys. **92**, 5057 (1990).

[21] S. Plimpton, J. Comp. Phys. **117**, 1 (1995).

[22] M. Pütz, K. Kremer, and G. S. Grest, Euro. Phys. Lett. **49**, 735 (2000), the simulations in this paper used a purely repulsive interaction between non-bonded monomers and a FENE interaction between bonded monomers. The N_e for this model is expected to be very similiar to that of the model used in the present study.

[23] H. R. Brown and T. P. Russell, Macromolecules **29**, 798 (1996).